J Mater Sci (2009) 44:4321–4325
DOI 10.1007/s10853-009-3644-z

Ferroelectric properties of $(1 - x)Bi(Zn_{1/2}Ti_{1/2})O_3$–$xPbZrO_3$ ceramics

O. Khamman · X. Tan · S. Ananta · R. Yimnirun

Received: 30 March 2009 / Accepted: 26 May 2009 / Published online: 9 June 2009

Abstract The $(1 - x)Bi(Zn_{1/2}Ti_{1/2})O_3$–$xPbZrO_3$ solid solution ceramics were prepared by using solid-state reaction method, and their ferroelectric properties were investigated. It was found that the perovskite structure is stable for compositions with $x \geq 0.900$. Within this composition range, the crystal structure of the solid solution preserves the orthorhombic symmetry of $PbZrO_3$ (PZ). The Curie point of the ceramics was found to decrease with increasing $Bi(Zn_{1/2}Ti_{1/2})O_3$ (BZT) content. The intermediate ferroelectric phase of PZ was stabilized by BZT addition and exists within a much wider temperature range in the solid solution.

Introduction

$Bi(Zn_{1/2}Ti_{1/2})O_3$ (BZT) is a unique lead-free ferroelectric compound with a tetragonal perovskite structure [1]. It is characterized by an extremely large *c/a* ratio of 1.21 and a high spontaneous polarization P_S of 103 μC/cm^2. Unfortunately pure BZT ceramic can only be formed under high pressures. Under ambient conditions, BZT ceramic decomposes to non-perovskite phases at 550 °C [1]. Recently, tetragonal perovskite $PbTiO_3$ (PT) and $BaTiO_3$ (BT) have been reported to be capable of stabilizing BZT at ambient conditions through solid solutions [2–7]. The uniqueness of BZT is also manifested in these solid solutions. In the $(1 - x)$BZT–xPT system, both the tetragonality and the Curie point increase with increasing amount of BZT and no morphotropic phase boundary (MPB) was observed [2, 4]. In particular, the composition 0.40BZT–0.60PT exhibits a high *c/a* ratio of 1.11 and a high Curie point exceeding 700 °C. In sharp contrast, decreases in the tetragonality and the Curie point was reported in the $(1 - x)$BZT–xBT solid solution [7]. Furthermore, an MPB was observed at $x \approx 0.90$ and a rhombohedral phase appeared with further increase in BZT. The paraelectric/ferroelectric transition becomes very diffuse with increasing amount of BZT, and the temperature for this transition is a minimum at the MPB composition.

$PbZrO_3$ (PZ) is the classic antiferroelectric (AFE) compound and is the end member in the solid solution with PT for the most widely used piezoelectric ceramics. At temperatures below 220 °C, PZ displays an orthorhombic perovskite structure with antiparallel shifts of Pb^{2+} ions along the pseudocubic ⟨110⟩ direction, which leads to the AFE behavior [8, 9]. The space group for the low temperature AFE phase was determined to be *Pbam* [10, 11]. At temperatures above 230 °C, PZ is in the paraelectric phase with the cubic *m3m* symmetry [9]. In-between the AFE and the paraelectric phase within a narrow temperature range, there is an intermediate phase which is arguably ferroelectric [9, 12, 13]. The temperature window for this intermediate ferroelectric phase was reported to be increased by forming solid solutions with $Pb(Ni_{1/3}Nb_{2/3})O_3$ [14, 15].

In this study, PZ is used to stabilize BZT at ambient conditions through forming the solid solution of $(1 - x)$

O. Khamman · S. Ananta · R. Yimnirun
Department of Physics, Faculty of Science, Chiang Mai University, Chiang Mai 50200, Thailand

X. Tan (✉)
Department of Materials Science and Engineering, Iowa State University, Ames, IA 50011, USA
e-mail: xtan@iastate.edu

BZT–xPZ, with focuses on the effect of BZT addition on the phase transitions and ferroelectric properties of PZ.

Experimental procedure

Ceramics of $(1 - x)$BZT–xPZ with $x = 0.900$, 0.925, 0.950, 0.975, and 1.000 were prepared with the conventional mixed-oxide method. Powders of Bi_2O_3 (99.9%), ZnO (99.99%), TiO_2 (99.9%), PbO (99.99%), and ZrO_2 (99.9%) were used as starting raw materials. After milled for 4 h with yttrium-stabilized zirconia media in ethanol, the powder was calcined at 900 °C for 2 h. Then the calcined powder was milled again and uniaxially pressed into disks at 150 MPa using 2 wt% polyvinyl alcohol as binder. Following binder burnout at 500 °C, the pellets were sintered in sealed crucibles between 1180 and 1200 °C for 2–10 h.

The density of the sintered ceramics was measured by the Archimedes method. The phase formation of the sintered specimens was analyzed by an X-ray diffractometer. For electrical property characterizations, the sintered pellets were ground and electrode with sputtered silver. During the dielectric permittivity measurement, the samples were heated from room temperature at a rate of 3 °C/min. The polarization hysteresis measurement was carried out with a standardized ferroelectric test system with a frequency of about 4 Hz.

Results and discussion

X-ray diffraction on the sintered pellets revealed that phase pure perovskite ceramics can be achieved in the $(1 - x)$ BZT–xPZ solid solution with x down to 0.900. Further increase in BZT inevitably leads to significant amounts of impurity phases. The X-ray diffraction patterns from phase pure ceramics with $x = 0.900$, 0.925, 0.950, 0.975, and 1.000 are shown in Fig. 1. Ceramics of these compositions display an orthorhombic perovskite structure that is isostructural to PZ. The lattice parameters of the orthorhombic structure for the ceramics are presented in Table 1. It is seen that the unit cell volume increases with composition x in the $(1 - x)$BZT–xPZ solid solution system. This trend is consistent with the fact that Pb^{2+} (1.49 Å) has a larger radius than Bi^{3+} (1.35 Å), whereas Zr^{4+} (0.72 Å) is bigger than the average radius of Zn^{2+} (0.74 Å) and Ti^{4+} (0.605 Å) [16]. These phase pure ceramics were found to have a high relative density, as also listed in Table 1.

The dielectric constant as a function of temperature measured at 1 kHz for the $(1 - x)$BZT–xPZ ceramics is shown in Fig. 2. The dielectric constant at the peak (ε_m) increases while the Curie point (T_C) decreases when BZT is incorporated into PZ. The values of ε_m and T_C for the ceramic series are listed in Table 2 for direct comparison. The decrease in T_C in $(1 - x)$BZT–xPZ ($x \geq 0.900$) is similar to that in $(1 - x)$BZT–xBT in the same

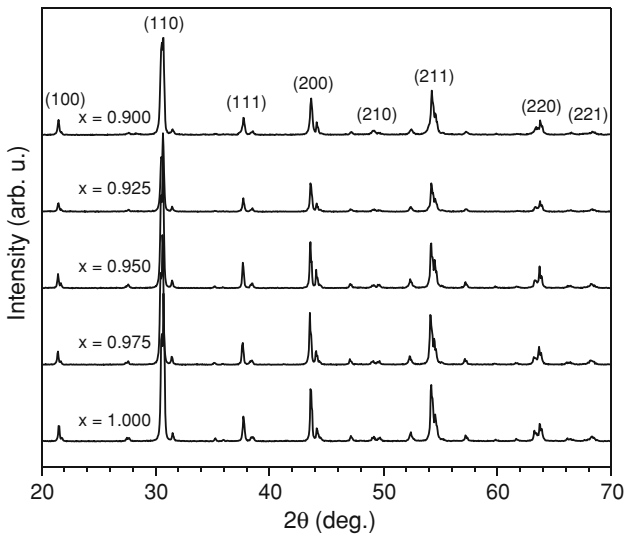

Fig. 1 X-ray diffraction patterns of the sintered $(1 - x)$BZT–xPZ ceramics. The peaks are indexed with the pseudocubic perovskite structure

Table 1 Density and unit cell dimensions of the sintered $(1 - x)$ BZT–xPZ ceramics

x	a (Å)	b (Å)	c (Å)	Unit cell volume (Å^3)	Relative density (%)
0.900	5.830	11.711	8.207	560.37	92
0.925	5.837	11.703	8.223	561.75	92
0.950	5.845	11.727	8.212	562.87	94
0.975	5.852	11.724	8.230	564.63	93

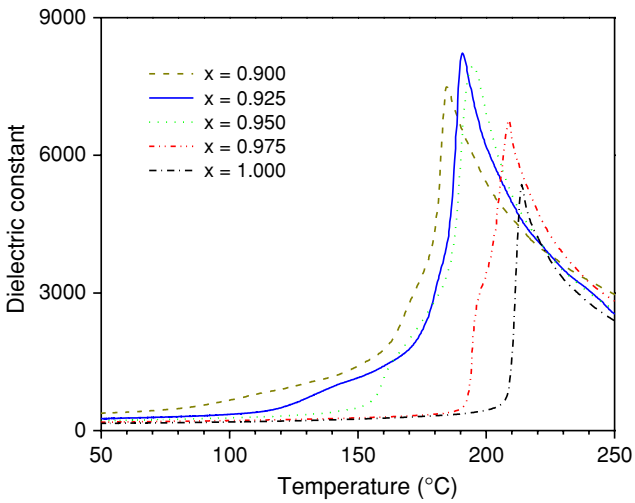

Fig. 2 Dielectric constant as a function of temperature measured at 1 kHz during heating in the $(1 - x)$BZT–xPZ ceramics

Table 2 Dielectric properties of the $(1 - x)$BZT–xPZ ceramics (at 1 kHz)

x	ε_m	T_C (°C)	T_F (°C)	$(T_C - T_F)$ (°C)
0.900	7500	185	77	108
0.925	8230	191	110	81
0.950	7950	195	153	42
0.975	6770	209	191	18

composition range [7]. Also evident in Fig. 2 is the widening of the temperature range for the intermediate phase when BZT is incorporated. The temperature window for this intermediate phase can be better seen from the dielectric loss tangent data shown in Fig. 3. The intermediate phase has a much higher dielectric loss than both the low temperature AFE phase and the high temperature paraelectric phase. The lower temperature boundary for this intermediate phase, denoted as T_F, is determined as the onset temperature for the dielectric loss increase during heating and is listed in Table 2. It is evident that T_F decreases much faster than T_C when the content of BZT increases in the solid solution. As a result, the temperature window $(T_C - T_F)$ widens significantly as BZT is incorporated into PZ. It is interesting to notice that the dielectric response of the intermediate phase displays a slight frequency dispersion. The observed widening of the temperature window, much higher dielectric loss, and the frequency dispersion of the intermediate phase in the $(1 - x)$BZT–xPZ solid solution bear the characteristics of the intermediate phase in the $(1 - x)Pb(Ni_{1/3}Nb_{2/3})O_3$–$x$PZ system we reported previously [14, 15].

The polarization hysteresis loop data for the $(1 - x)$BZT–xPZ ceramics at room temperature are shown in Fig. 4. It is found that with increasing content of BZT, the slope increases and the hysteresis loop gradually opens up. In particular, the ceramic of composition $x = 0.900$ even displays a small remanent polarization (0.5 μC/cm^2) at room temperature. Considering the fact that the lower temperature limit (T_F) for the intermediate phase shifts toward room temperature when BZT content increases, the increase in the remanent polarization seems to suggest that the intermediate phase is of ferroelectric nature.

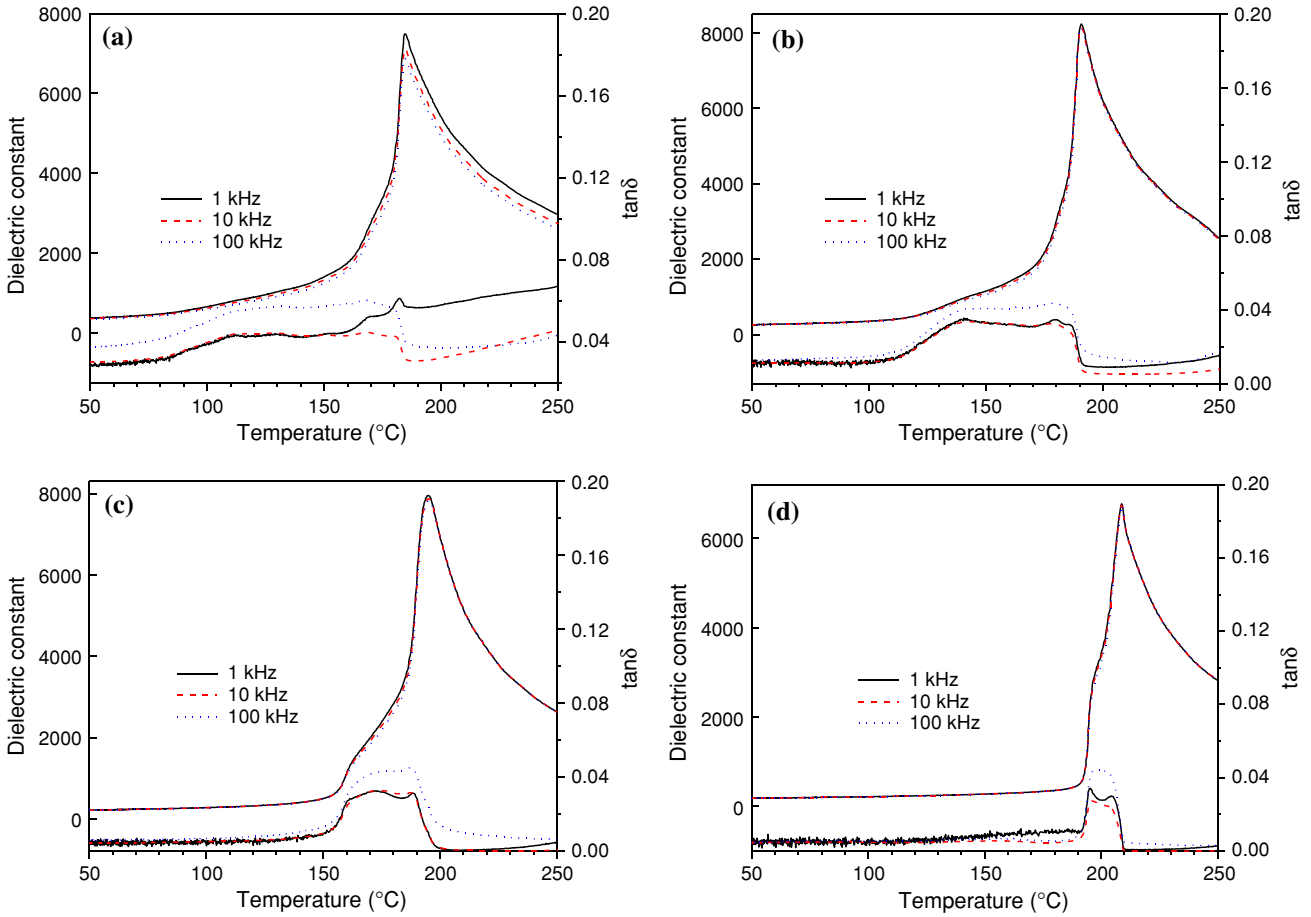

Fig. 3 Temperature and frequency dependences of dielectric constant and loss tangent tan δ in the $(1 - x)$BZT–xPZ ceramics. **a** $x = 0.900$, **b** $x = 0.925$, **c** $x = 0.950$, and **d** $x = 0.975$

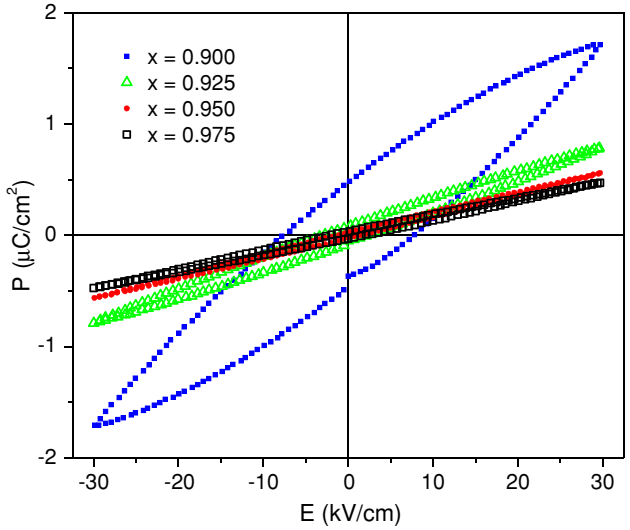

Fig. 4 Polarization versus electric field hysteresis loops measured at room temperature at 4 Hz in the $(1 - x)$BZT–xPZ ceramics

The ferroelectric nature of the intermediate phase is confirmed by the polarization hysteresis loop data at higher temperatures (Fig. 5). Under the fixed peak field of 30 kV/cm, the ceramic with composition $x = 0.900$ displays a well-defined hysteresis loop at 80 °C with a remanent polarization P_r of 21.3 μC/cm^2. Increasing temperature further leads to a decrease in the coercive field E_c. In contrast, a very slim loop was recorded at 60 °C. The ceramic with composition $x = 0.925$ started to display a well-defined hysteresis loop at 120 °C with a P_r of 28.4 μC/cm^2, whereas the ceramic of $x = 0.950$ started at 160 °C with a P_r of 29.5 μC/cm^2. The ceramic of $x = 0.975$ maintains a slim loop with a negligible P_r under the peak field of 30 kV/cm up to 160 °C. It should be noted from Table 2 that T_F is 77, 110, 153, and 191 °C for compositions $x = 0.900$, 0.925, 0.950, and 0.975, respectively. Therefore, the hysteresis loop data are consistent with the results from the dielectric permittivity measurement. The results directly support that the intermediate phase between the high temperature paraelectric and the low temperature AFE phase is of ferroelectric nature.

Conclusions

Single phase perovskite ceramics in the $(1 - x)$BZT–xPZ solid solution system can be synthesized with the conventional mixed oxide method for $x \geq 0.900$. Incorporating BZT into PZ shifts the Curie point T_C to lower temperatures, increases the maximum dielectric constant ε_m, and stabilizes the intermediate phase. The intermediate phase between the high temperature paraelectric and the low temperature AFE phase is ferroelectric and is characterized

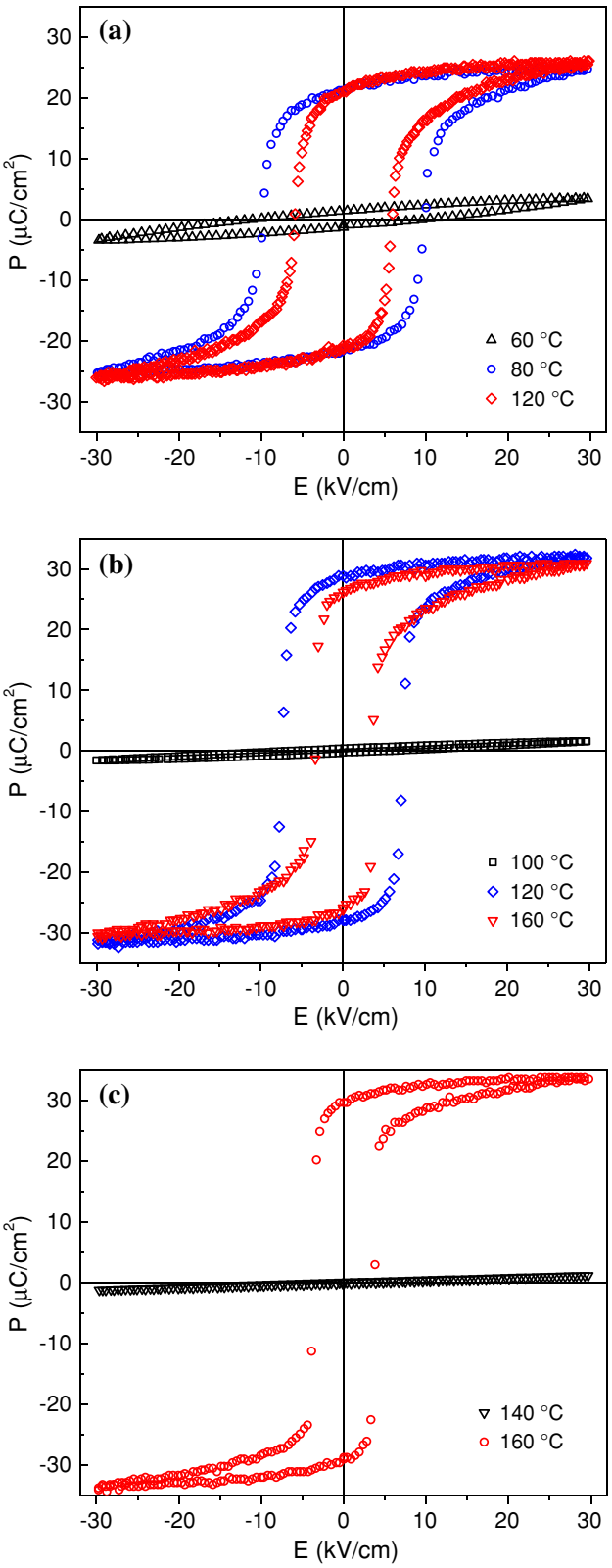

Fig. 5 Polarization hysteresis loops measured at 4 Hz during heating at a series of temperature in the $(1 - x)$BZT–xPZ ceramics. **a** $x = 0.900$, **b** $x = 0.925$, and **c** $x = 0.950$

by a significantly higher dielectric loss, a slight frequency dispersion in the dielectric response, and well-defined hysteresis loops with high remanent polarizations.

Acknowledgements This study was supported by the National Science Foundation through the CAREER Grant DMR-0346819 and the Thailand Research Fund (TRF), the Commission on Higher Education (CHE), and the Faculty of Science, Chiang Mai University, Thailand.

References

1. Suchomel MR, Fogg AM, Allix M, Niu H, Claridge JB, Rosseinsky MJ (2006) Chem Mater 18:4987
2. Suchomel MR, Davies PK (2005) Appl Phys Lett 86:262905
3. Grinberg I, Suchomel MR, Dmowski W, Wojtek SE, Wu H, Davies PK, Rappe AM (2007) Phys Rev Lett 98:107601
4. Zhang XD, Kwon D, Kim BG (2008) Appl Phys Lett 92:082906
5. Kwon D, Kim B, Tong P, Kim BG (2008) Appl Phys Lett 93:042902
6. Huang CC, Cann DP, Tan X, Vittayakorn N (2007) J Appl Phys 102:044103
7. Huang CC, Cann DP (2008) J Appl Phys 104:024117
8. Sawaguchi E, Maniwa H, Hoshino S (1951) Phys Rev 83:1078
9. Viehland D (1995) Phys Rev B 52:778
10. Corker DL, Glazer AM, Dec J, Roleder K, Whatmore RW (1997) Acta Crystallogr B53:135
11. Teslic S, Egami T (1998) Acta Crystallogr B54:750
12. Xu Z, Dai X, Viehland D, Payne DA (1995) J Am Ceram Soc 78:2220
13. Tanaka M, Saito R, Tsuzuki K (1982) Jpn J Appl Phys 21:291
14. Wirunchit S, Vittayakorn N (2008) J Appl Phys 104:024103
15. Qu W, Tan X, Vittayakorn N, Wirunchit S, Besser MF (2009) J Appl Phys 105:014106
16. Shannon RD (1976) Acta Crystallogr A32:751